PNAS
Proceedings of the National Academy of Sciences of the United States of America www.pnas.org

Supporting Information

Twenty-first Century Megapolitan Expansion - Rolling Back Warming with Urban Adaptation Strategies

M. Georgescu*, P. Morefield, B. G. Bierwagen, C. P. Weaver

*To whom correspondence should be addressed. E-mail: matei.georgescu@asu.edu

This file includes:

Materials and Methods

Modeling

WRF has a detailed level of complexity, including multiple parameterization options for the land surface, boundary layer, convection, microphysics, and radiation (1). Preliminary model simulations were conducted to benchmark code stability and performance (i.e., correspondence to observed climate). This resulted in the selection of the following parameterization options, presented in Table S2.

The three-category UCM (2, Table S2) required diurnal profiles of anthropogenic heating (AH) for each of the low, medium, and high intensity residential/commercial urban classes. The peak daytime values of AH utilized for all simulations were 20, 30, and 35 Wm^{-2} in order from least to most intense urban classification. Maximum AH values utilized correspond to a metropolitan area with a conservative contribution of heating from anthropogenic sources (3-4). The hourly factor applied to AH (with peak values as expressed above), which expresses the fraction of hourly AH emission, starting at 01 Local Time through the end of the 24-hour diurnal cycle (this factor was applied for each hour of the simulated period, for all urban areas) is presented in *Fig. S1*. Also shown are diurnal AH representations (after multiplication by the aforementioned factor with daytime AH maxima) for each of the above-mentioned urban classes. Two maxima are evident, corresponding to heating due to traffic patterns, which rise during morning rush hour and once again during late-afternoon/evening hours. Additional components contributing to the diurnal shape of the AH pattern are electricity consumption and human metabolism (the latter of which is a second-order AH contributor; 4). The diurnal shape of AH profiles is consistently similar across a select number of large cities across the United States (4), with differences arising from the magnitude of AH contribution. The AH magnitude utilized for our simulations, more similar to Los Angeles than Philadelphia, therefore indicate a conservative AH contribution to future urban expansion, since the identical AH profiles presented in *Fig. S1* were utilized for both current and future urban expansion/adaptation scenarios.

For non-urban classes, a Moderate Resolution Imaging Spectroradiometer-based 20-category land use and land cover classification with modifications by NCEP (1) was used to represent the remaining land surface portion of the modeling domain (see also: ftp://ftp.emc.ncep.noaa.gov/mmb/gcp/ldas/noahlsm/README). Urban area representation made use of the Environmental Protection Agency's Integrated Climate and Land Use Scenarios Project (ICLUS version 1.3; 5), which produced spatially resolved scenarios of current and future urban expansion, consistent with projections of global change. ICLUS projections were mapped to the WRF domain, with Control experiments using modern day urban representation (5) representative of year 2000, consistent with the time period of Control simulations. Projected changes in urban expansion were categorized according to the degree of expansion, with A2 ICLUS corresponding to greatest expansion and B1 ICLUS corresponding to least urban expansion for year 2100 (*Table S1*).

We represent albedo (for all non-urban classes) based on a monthly, five-year, 0.144°

climatological dataset assumed to be valid at the 15th of each month (6). Monthly vegetation fraction (i.e., the fraction of each 20-km grid cell that is not bare soil) fields, for non-urban classes, are based on a five-year, 0.144° climatological dataset, with values in percentages ranging from 1 to 99 over land, and 0 over water (*7*).

All adaptation simulations were based on the A2 ICLUS urban expansion scenario for year 2100. A trio of adaptation strategies were examined (*Table S1*): (1) a green roofs approach (hereafter A2-GreenRoofs), (2) a cool roofs approach (hereafter A2-CoolRoofs), and (3) a hybrid approach incorporating biophysical characteristics of both cool and green roofs (hereafter A2-GreenAlbedo).

Incorporation of green roofs as an urban heat island (UHI) mitigation strategy has demonstrated multiple benefits ranging from storm water retention, to increased energy savings resulting from decreased temperatures, to air quality enhancement within the built environment (8-16). Our work extends previous research in two important ways. First, by focusing on large spatial scales (i.e., the entire United States) we are able to address the efficacy of this strategy across many urban environments simultaneously, facilitating capacity to examine geographical locations where this approach is optimal. Second, our green roofs implementation is dynamically coupled to WRF (i.e., green roofs operating within a larger scale numerical modeling framework), thereby allowing for process simulation of the fully interacting urban-regional climate environment including examination of potential feedbacks. To our knowledge, a fully explicit green roofs model has yet to be implemented within a dynamical climate model (e.g., WRF) and our aim here is to investigate maximum potential benefits that could be realized via the most basic implementation of this adaptation approach, encouraging future work integrating a fully explicit green roofs (and walls) parameterization that includes multiple roof soil layers as well as vegetation characteristics (e.g., LAI, albedo, etc.) and seasonally evolving phenology. To simplify and assess first-order impacts, we set roof moisture availability to a value corresponding to 1 mm of rain (i.e., we assume 1mm thick pool of water on all roofs) for all urban classes at all times. One drawback of this simple approach is that while we are able to examine maximum hydroclimatic impacts associated with the green roofs strategy, we are not able to assess effects on air quality (as no vegetation is explicitly present in this preliminary implementation). Our assumption behind this approach is that a principal benefit of green roof strategies is derived from enhanced evapotranspiration (ET) due to vegetation, and resulting cooling impacts. Our approach therefore maximizes potential ET-derived benefits as the flux of water to the atmosphere is limited by insolation only (i.e., we assume water availability is not a constraint). In this manner, our GreenRoofs (*Table S1*) simulations account for the maximum possible hydroclimatic effects of green roof deployment.

The effectiveness of cool roofs is based on the premise of highly reflective materials, whereby a greater fraction of incoming solar radiation is not absorbed by rooftop surfaces (17). Previous research on the efficacy of cool roofs to decrease surface (or near-surface) temperatures has shown that temperatures can be lowered significantly, with considerable potential for energy savings (18-27), an especially important consideration for already large or rapidly expanding urban areas in warmer climates. More recently, potential

tradeoffs associated with large-scale deployment of cool roofs have been highlighted on global (28) and regional scales (29). Research addressing tradeoffs associated with large-scale cool roofs adoption (green roofs as well) is therefore necessary to examine location specific impacts on local to regional scales across climate zones to optimize maximal positive benefits. For our second urban adaptation approach (i.e., A2-CoolRoofs; *Table S1*), we set all roof albedos to EPA Energy Star SOLARFLECT coating value of 0.88, a value
lower than the initial reflectivity after set-up and appropriate after three years of wear and tear (EPA Energy Star roof product list: http://downloads.energystar.gov/bi/qplist/roofs_prod_list.pdf?8ddd-02cf). This was the highest EPA Energy Star roof albedo value available, highlighting our intention of examining maximum impacts associated with widespread deployment of various adaptation strategies, to quantify and contrast peak benefits and tradeoffs.

The final adaptation strategy examined (*Table S1*) was inspired by a recent bio-engineering approach aimed at maximizing solar reflectivity of crop varieties to mitigate surface warming due to long-lived emissions of greenhouse gases (30). Our modification of vegetation traits is a hybrid approach that assumes maximally transpiring *and* reflecting vegetation, combined into one rather than two separate approaches. An important question is how impacts due to cool roofs and green roofs scale when incorporating this hypothetical strategy, i.e., do integrated effects from cool roofs and green roofs scale linearly, or instead, is there a saturation rate beyond which impacts from such strategies no longer matter?

Evaluation of Control Experiments

Prior to examination of impacts due to urban expansion, the ability of WRF to accurately simulate United States climate during 2001-2008 must be demonstrated. The WRF Control simulation is evaluated against suitable gridded temperature and precipitation products.

First we make use of the University of Delaware Global Air Temperature dataset, a gridded temperature product available courtesy of the Earth Systems Research Laboratory (http://www.cdc.noaa.gov). All Control experiment ensemble members (*Table S1*) for 2001-2008 were averaged, and the resulting comparison is presented in *Figure S2* against the Delaware Global Air Temperature product for the equivalent time period.

WRF captures the seasonal evolution of near-surface temperature from spring through the winter season. Broad warming from spring to summer is apparent over most interior regions, with reduced warming over the higher terrain of the Rocky and Appalachian Mountains, and the Pacific and Atlantic coastlines, agreeing admirably with the Delaware Global Air Temperature dataset. There is a general warm bias of ~3-5°C for summer season (i.e., JJA) over the Great Plains, potentially related to simulated drying of the top soil layers during late spring/early summer season. Fall, winter, and spring season near-surface temperatures are reproduced with excellent fidelity, with negligible bias over any region of the lower 48 states. In general, both the magnitude and spatial variability of

near-surface temperature are well reproduced providing confidence in the model's ability to accurately simulate the diverse and seasonally varying thermal behavior of the United States during the simulated time period.

Researchers have recently emphasized that considerable variability exists among different precipitation datasets, compounding uncertainties associated with model simulation evaluation against gridded products (31). For this reason, WRF simulated precipitation is compared to a pair of observationally based, gridded products: (i) the University of Delaware Global Precipitation dataset, and (ii) the *CPC US Unified Precipitation dataset provided by NOAA/OAR/ESRL PSD from their Web site at* http://www.esrl.noaa.gov/psd/data/gridded/data.unified.html. Figure S3 compares Control performance (*Figure S3a*) to the Delaware (*Figure S3b*) and UNIFIED (*Figure S3c*) datasets. The UNIFIED dataset does not include data for Canada, and all pixels over the country were set to an undefined value. Our focus is therefore restricted to the continental United States, for which data availability does not restrict Control experiment evaluation, and which is the focus of the conducted sensitivity experiments.

Both gridded product datasets illustrate a distinct demarcation, generally along the 100th meridian, separating the relatively moister eastern from the relatively drier western United States. WRF properly simulates the position and magnitude (1.5–2 mm day^{-1}) of this boundary. The gridded products are in general agreement with one another over western portions of the United States, but differ from WRF Control simulations, which produce greater precipitation amounts along the higher terrain of the Rocky and Sierra Mountain ranges, as well as the Mogollon Rim and northern half of the Pacific coastline. Differences between the gridded products and the Control experiment are likely due to the higher resolution of WRF simulations, which better capture the variability of western United States terrain and coastline features. The Delaware product appears to be the driest of the pair of observationally based datasets, highlighting the value of evaluating model simulation results against more than one product. WRF is able to capture the tendency of enhanced precipitation across the Gulf States, a feature previously not well captured. As already mentioned for temperature, the magnitude and spatial variability of precipitation is well simulated, and provides further confidence in the model's ability to simulated United States climate during this period of time.

It is important to highlight that it is not the intent of this research to replicate 2001-2008 climate exactly, but to provide assurance that regional and large-scale features are ably reproduced in order to provide confidence in the tool for the sensitivity experiments under investigation. We expect that inherent model biases (e.g., summer-time warm bias over the Great Plains) are consistent across the suite of sensitivity simulations and consequently offset one another when calculating differences.

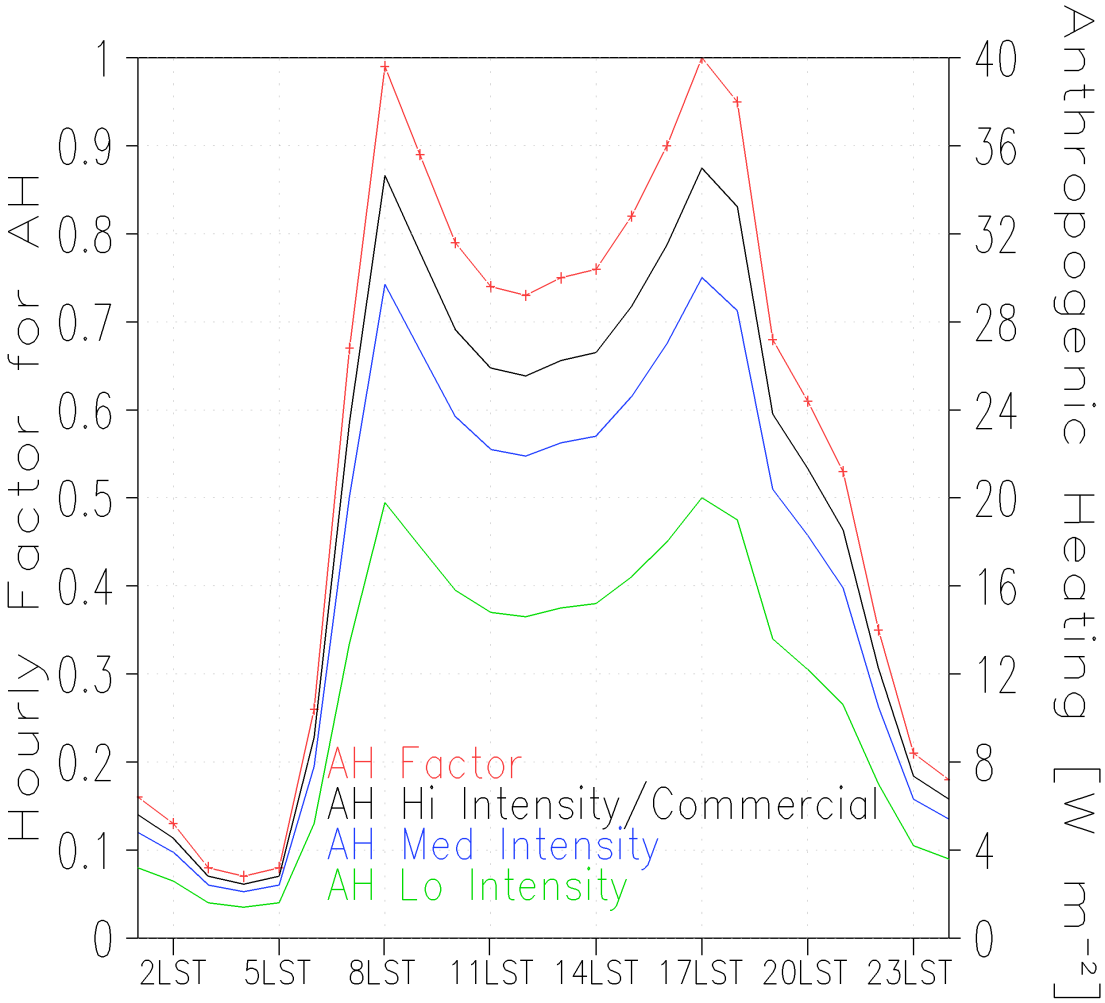

Fig. S1. Diurnal cycle of anthropogenic heating factor (red line with crosses) and UCM category-specific anthropogenic heating utilized for all simulations (AH High Intensity/Commercial: black line; AH Medium Intensity: blue line; AH Lo Intensity: Green line). Time shown is Local Time.

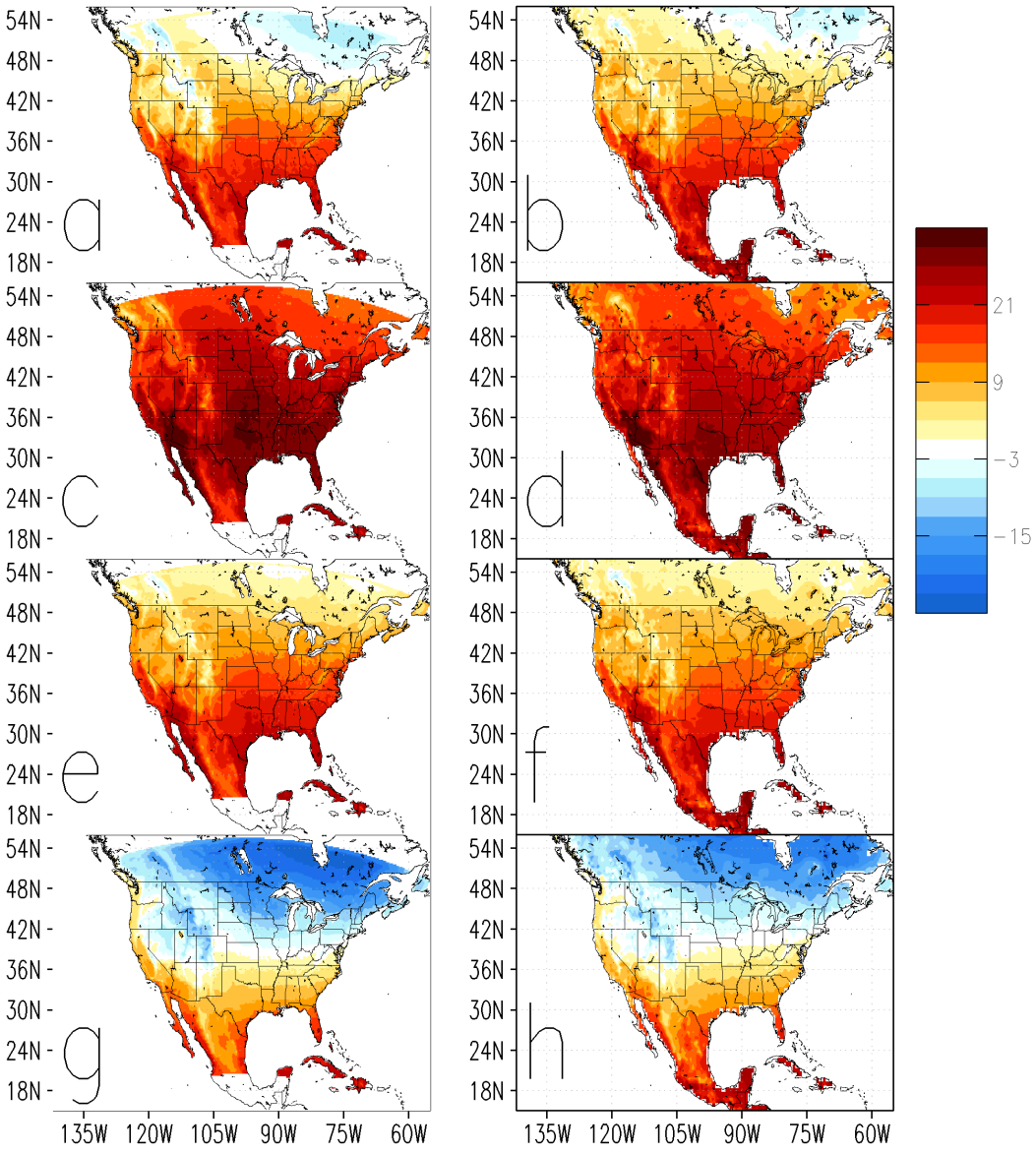

Fig. S2. Simulated (left hand column) and observed (right hand column) seasonally averaged 2m air temperature (°C), for **(a-b)** spring, **(c-d)** summer, **(e-f)** fall, and **(g-h)** winter, for Control experiments. Time period of all simulations is 2001-2008. Observational dataset used is the University of Delaware Global Temperature dataset.

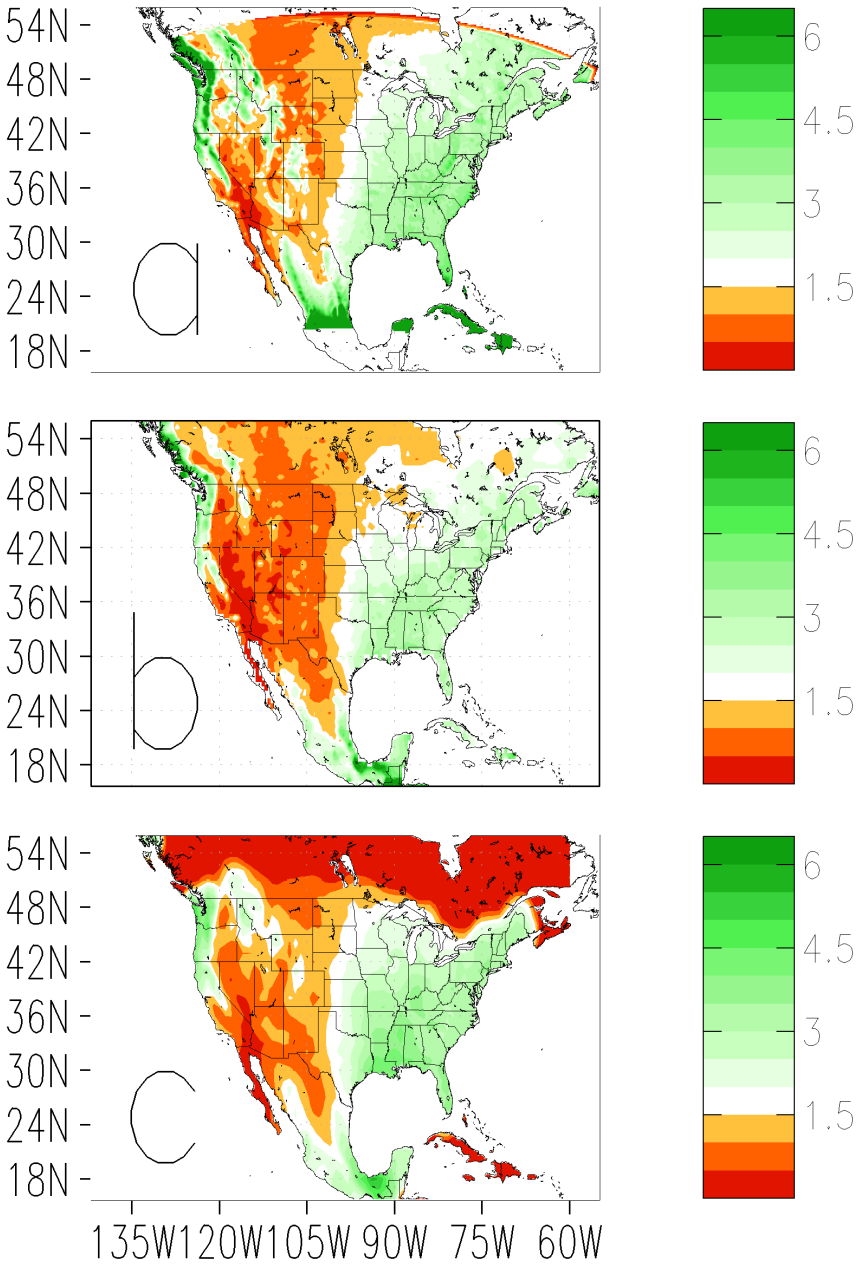

Fig. S3. Simulated and observed total accumulated precipitation, for **(a)** WRF Control simulation, **(b)** University of Delaware Global Temperature dataset, and **(c)** UNIFIED Precipitation dataset. Time period of analysis is 2001-2008. Units are mm day^{-1}.

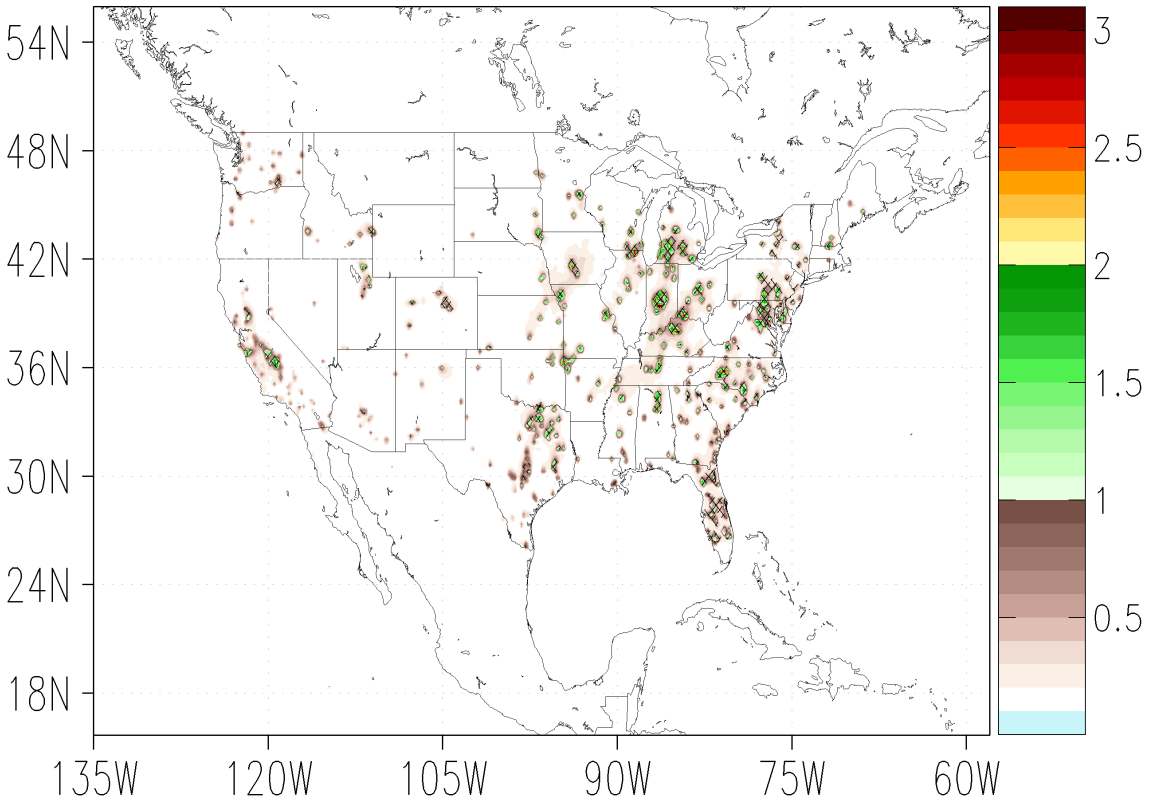

Fig. S4. As Figure 1, but for B1 ICLUS expansion scenario minus Control experiment (°C).

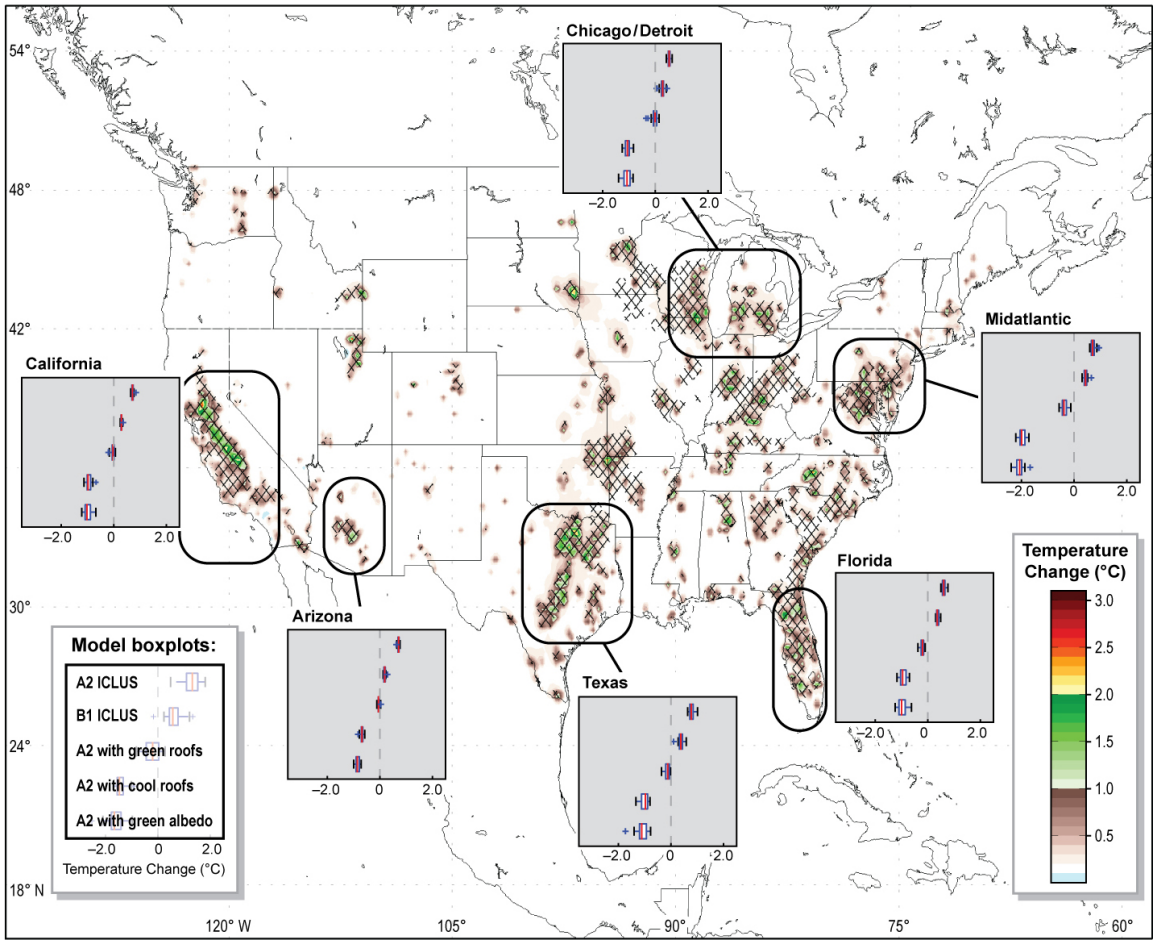

Fig. S5. As Figure 1, but for MAM.

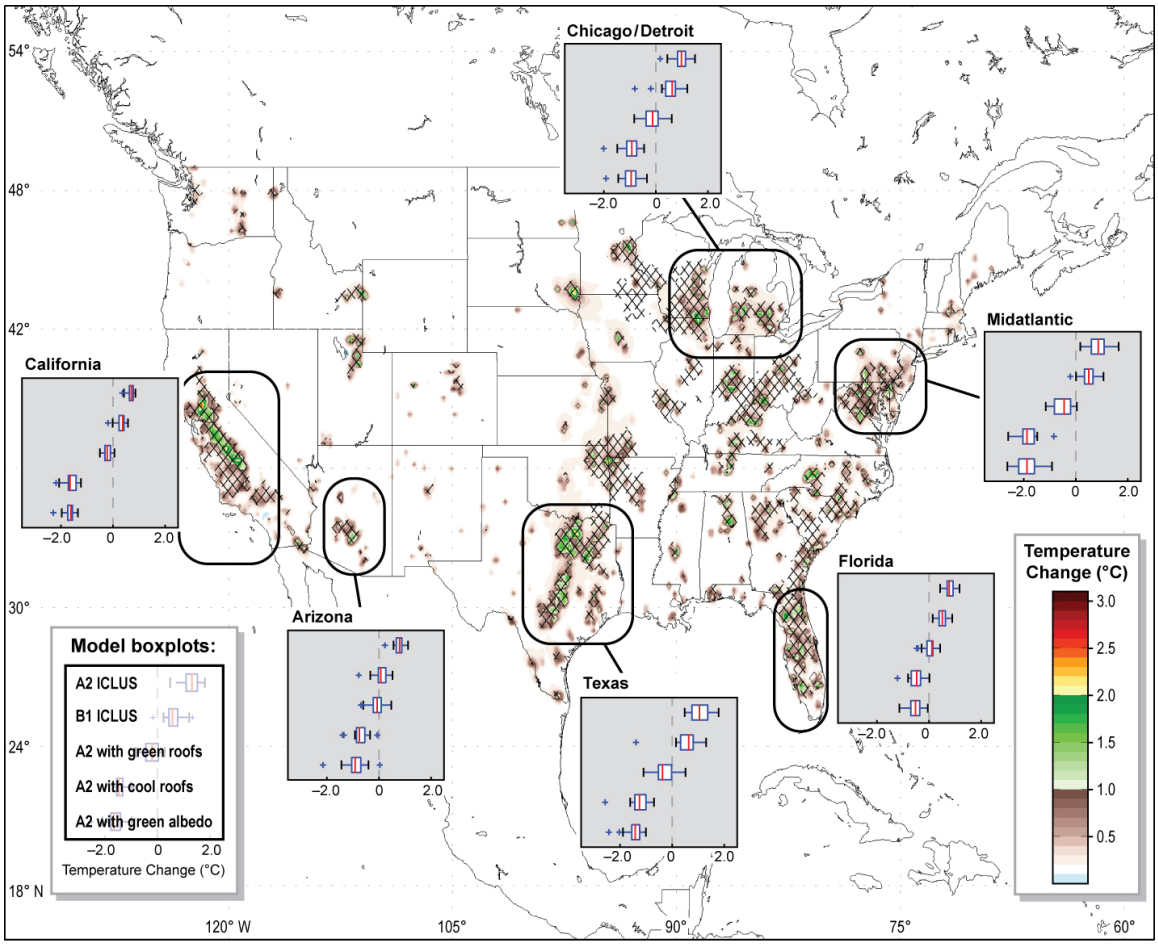

Fig. S6. As Figure 1, but for SON.

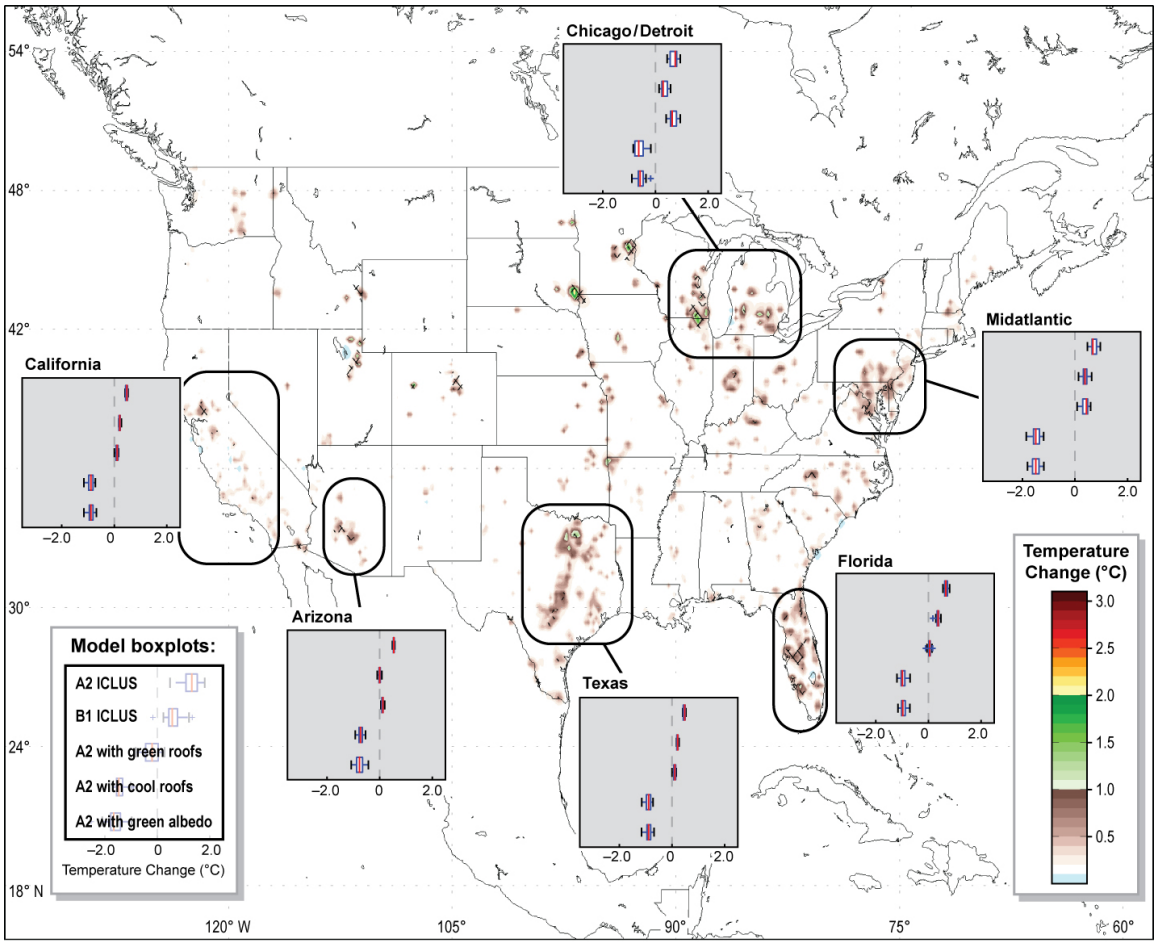

Fig. S7. As Figure 1, but for DJF.

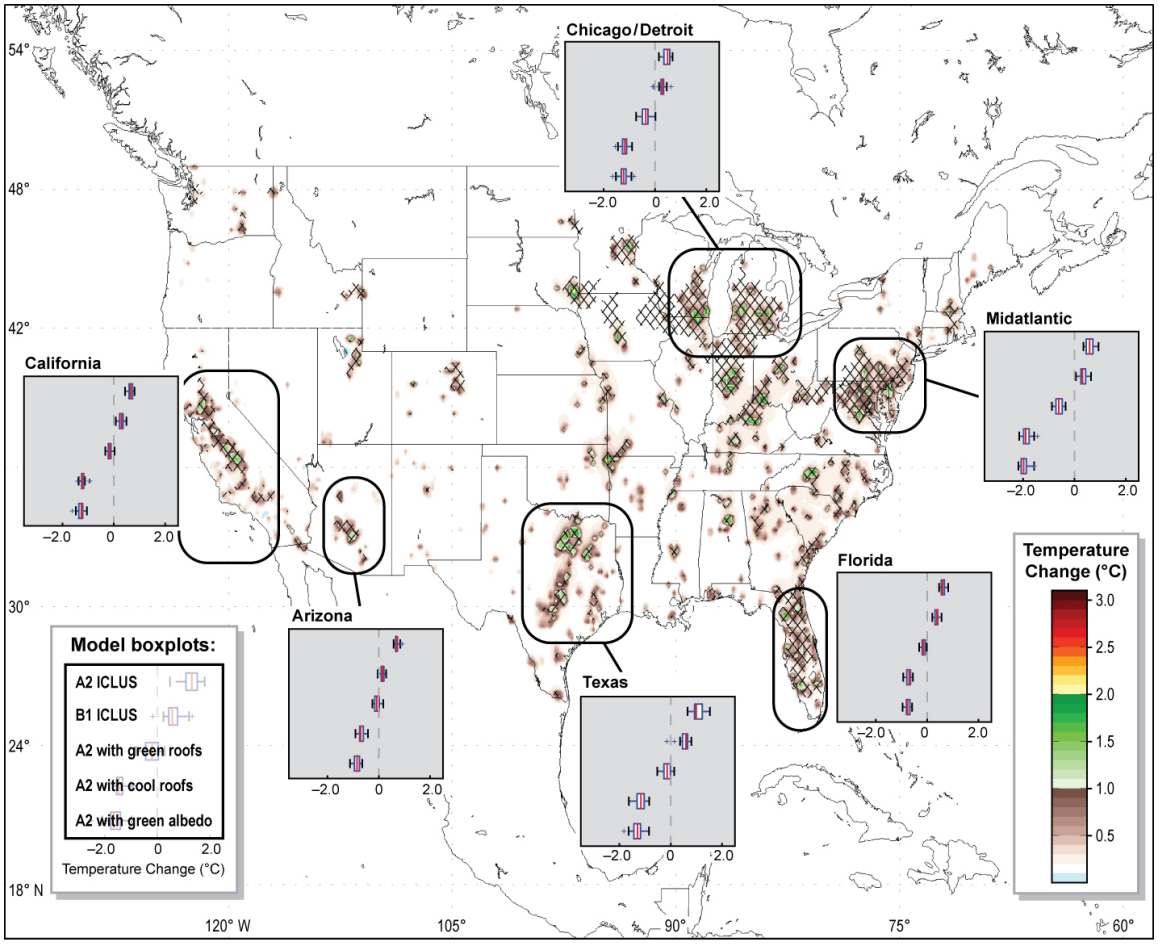

Fig. S8. As Figure 1, but for entire year.

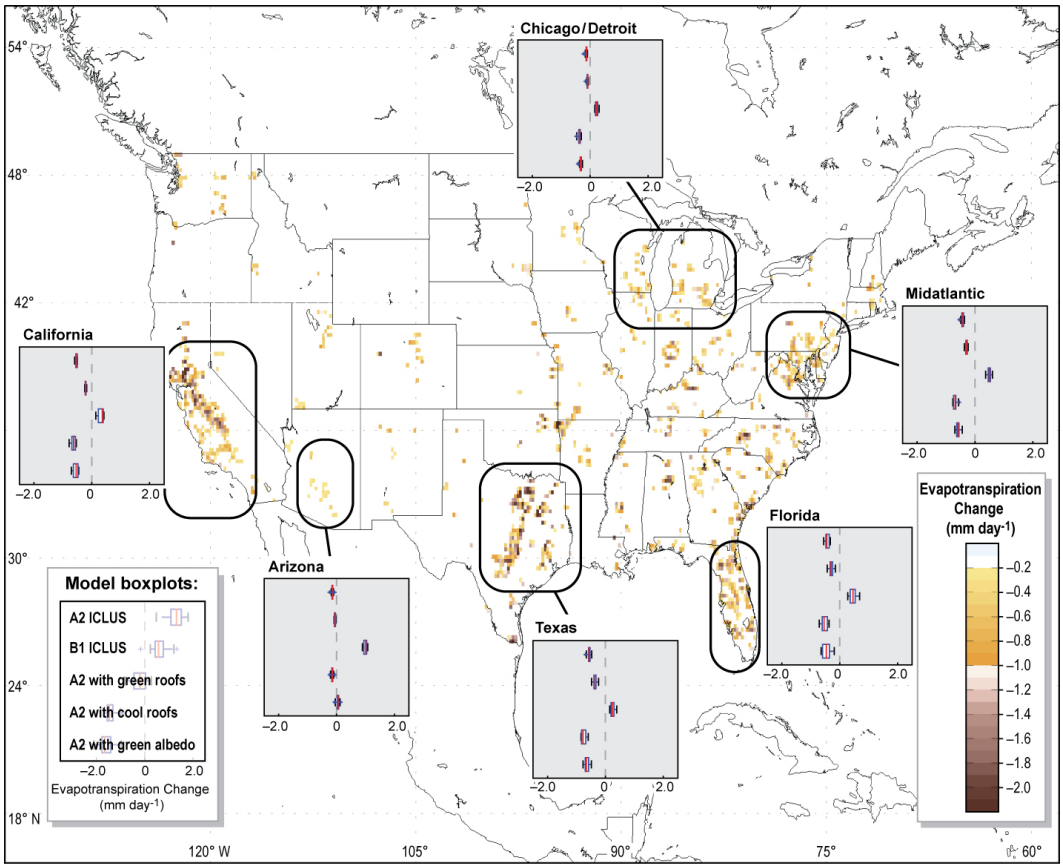

Fig. S9. Simulated March-April-May (MAM) evapotranspiration (ET) difference between A2 and Control (mm day^{-1}). Differences are shown only for statistically significant pixels (illustrated by hatching in Figure 1). Estimated impacts of all expansion and adaptation scenarios for indicated urban areas are shown as insets and performed only for statistically significant grid cells, with black ovals outlining each region. Red lines show median impacts; blue box bars show 1st and 3rd quartiles and whiskers represent endpoints, from 24 simulated summers. box plots indicate differences between A2 and control, B1 and control, A2 green roofs and control, A2 cool roofs and control, and A2 with green–albedo roofs and control from top to bottom, respectively.

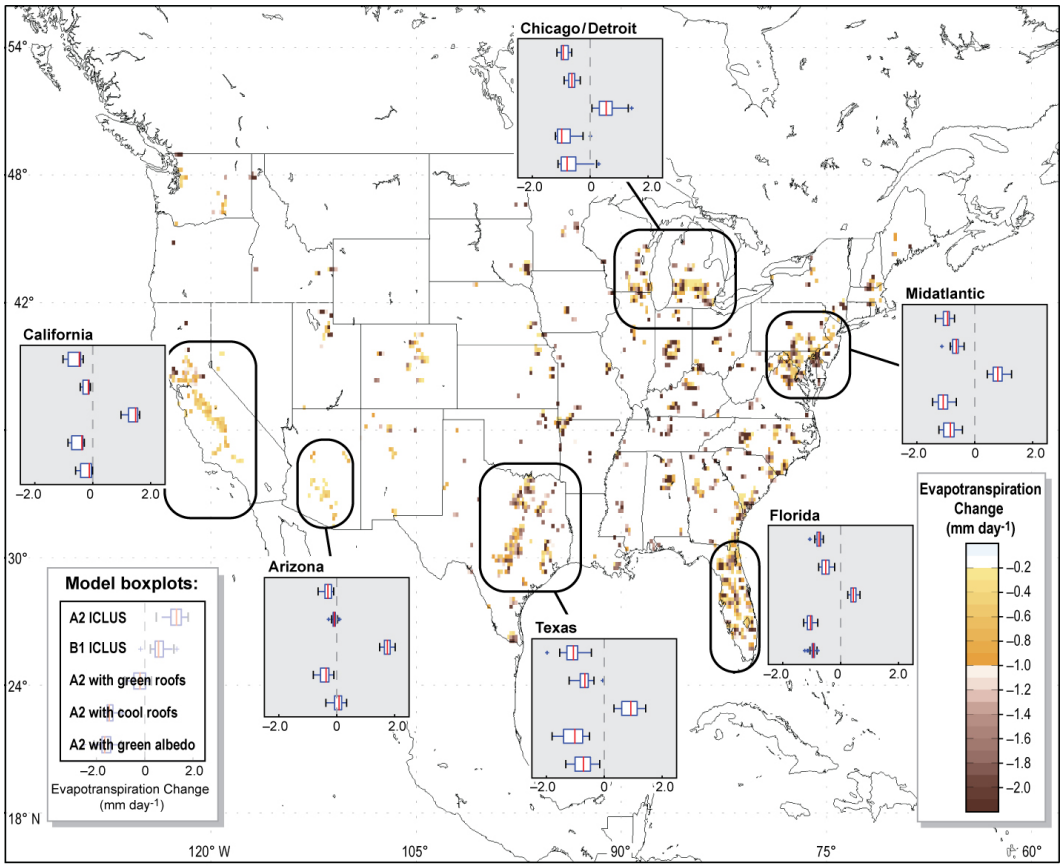

Fig. S10. As Figure Fig. S9 but for JJA.

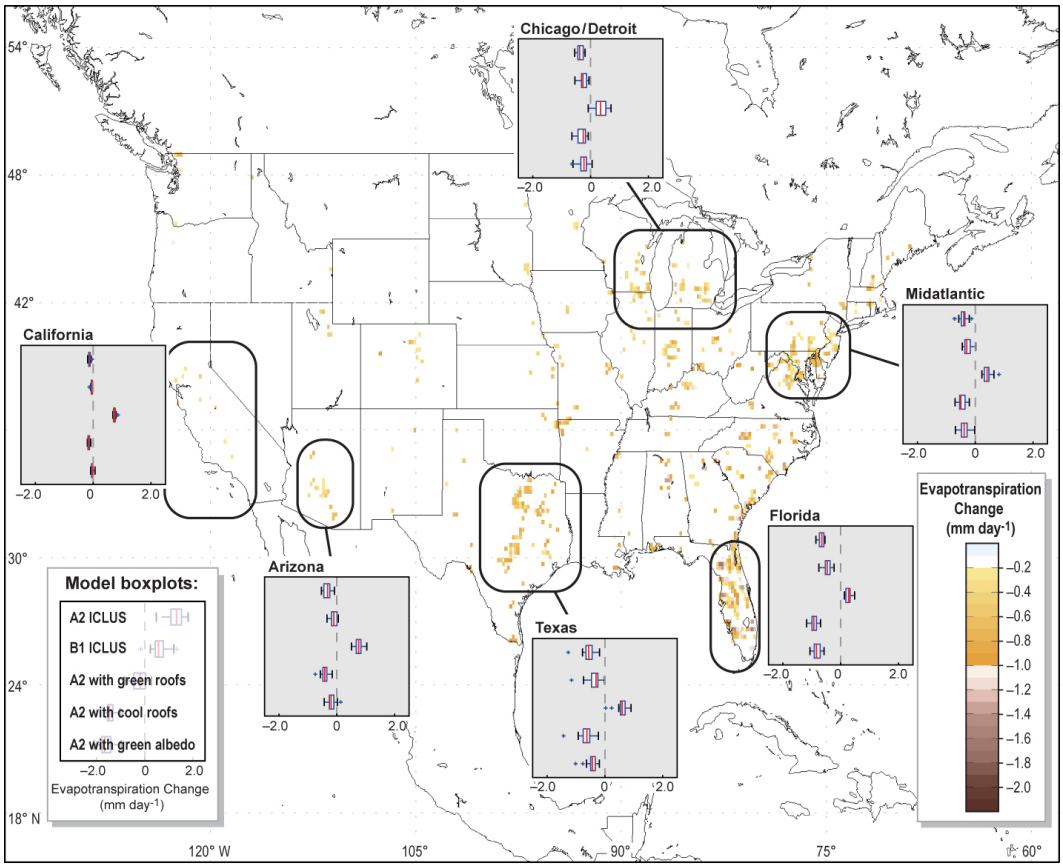

Fig. S11. As Figure Fig. S9 but for SON.

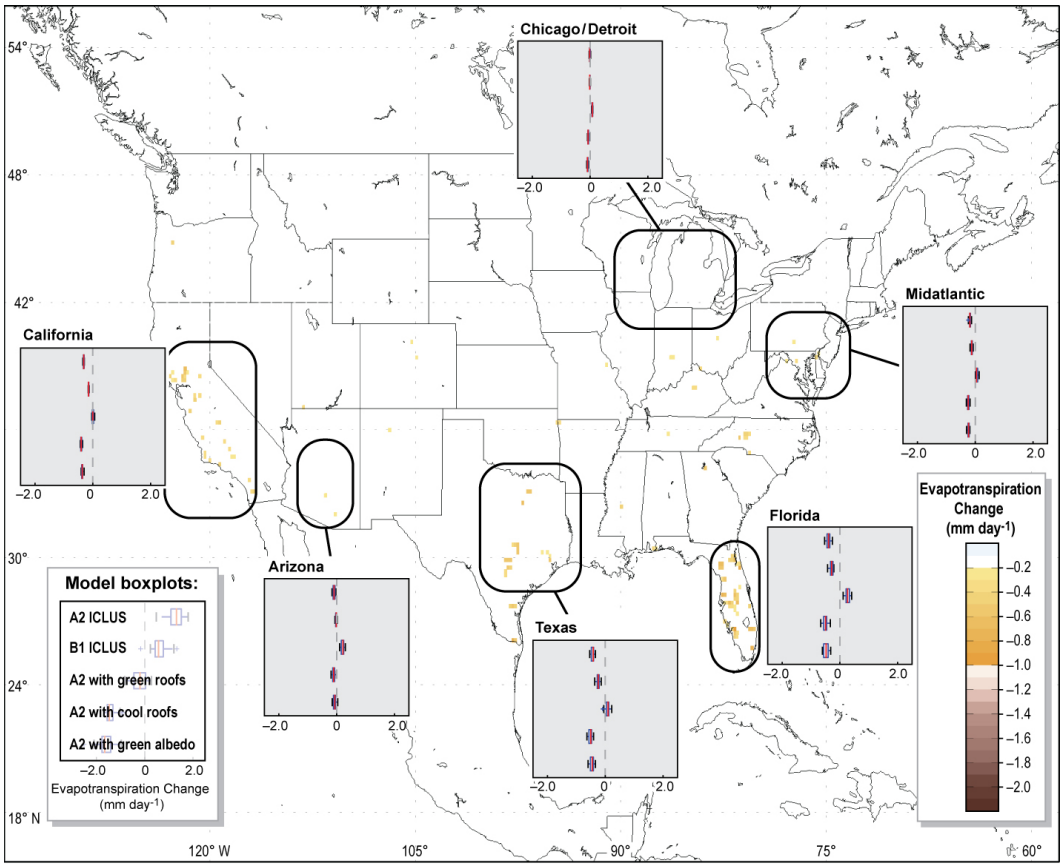

Fig. S12. As Figure ET for DJF.

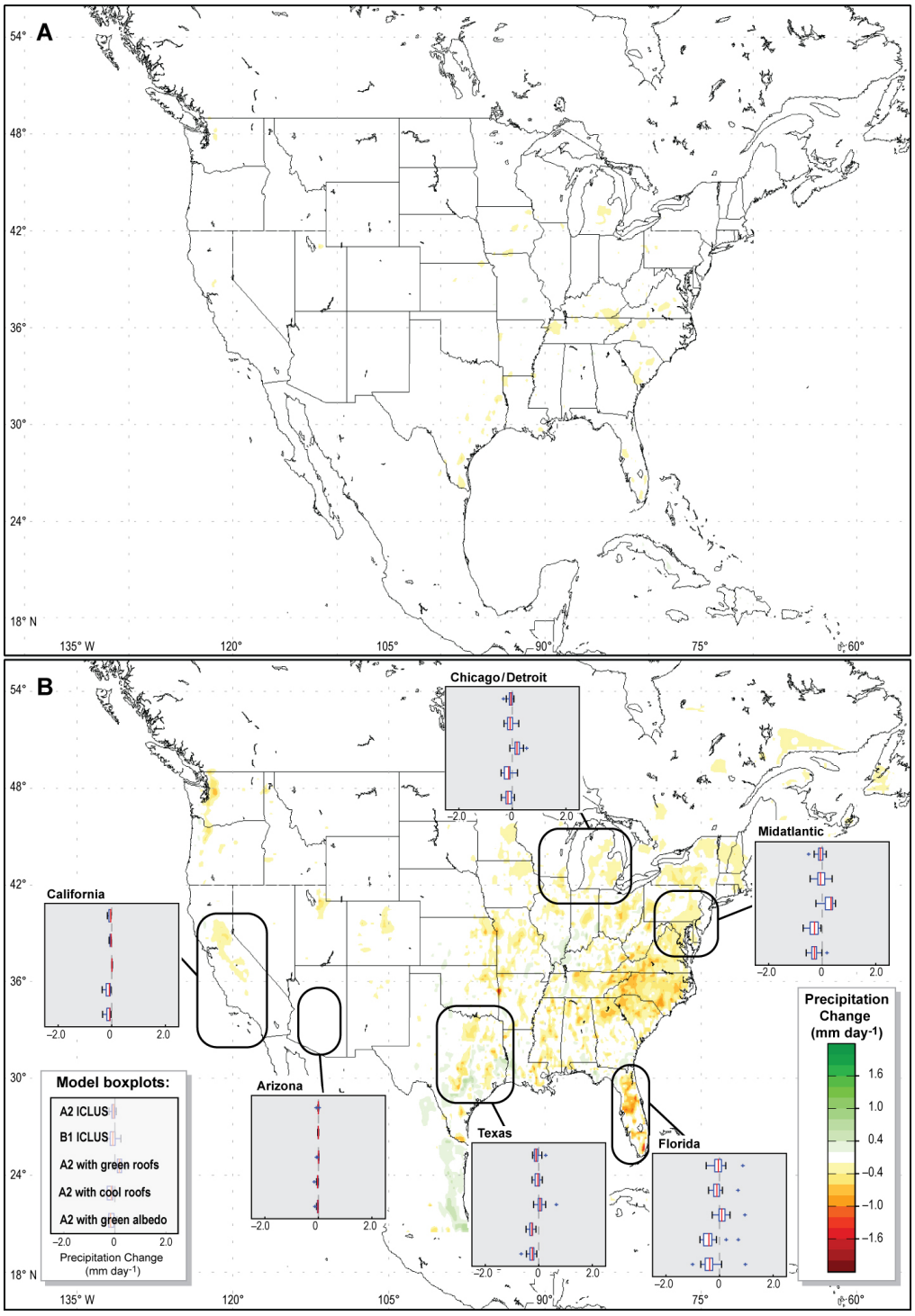

Fig. S13. As Figure 2 but for MAM.

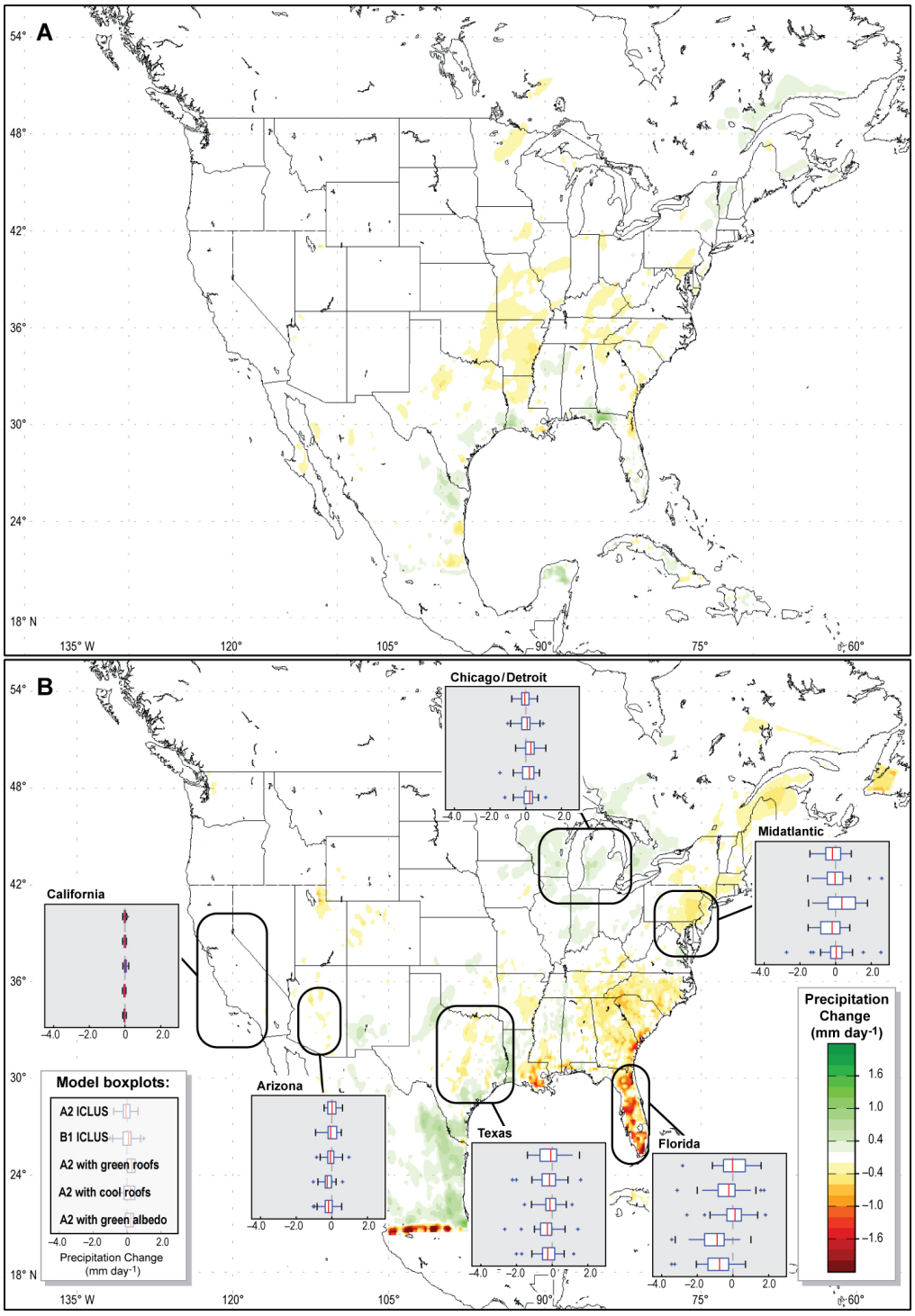

Fig. S14. As Figure 2 but for SON.

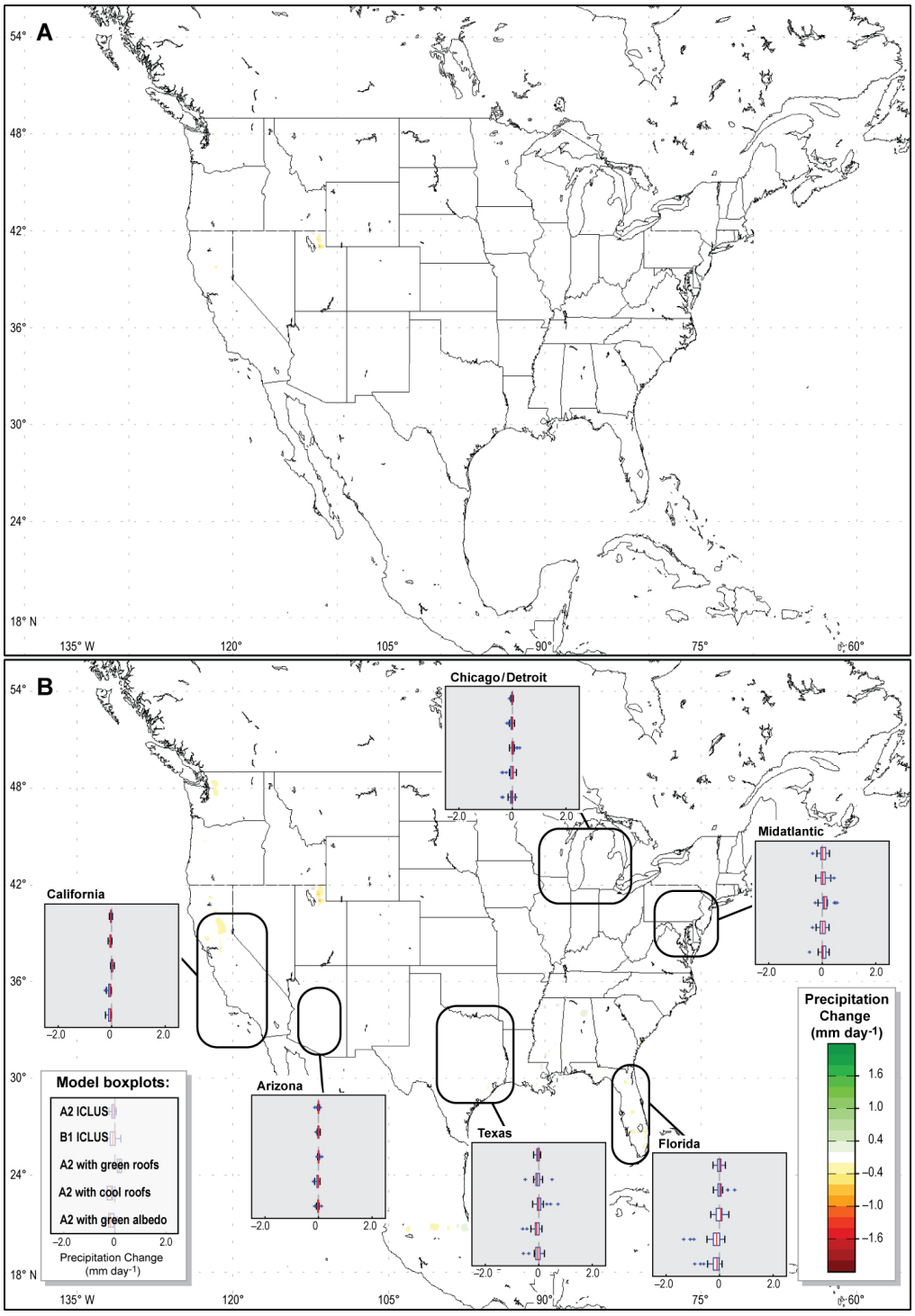

Fig. S15. As Figure 2 but for DJF.

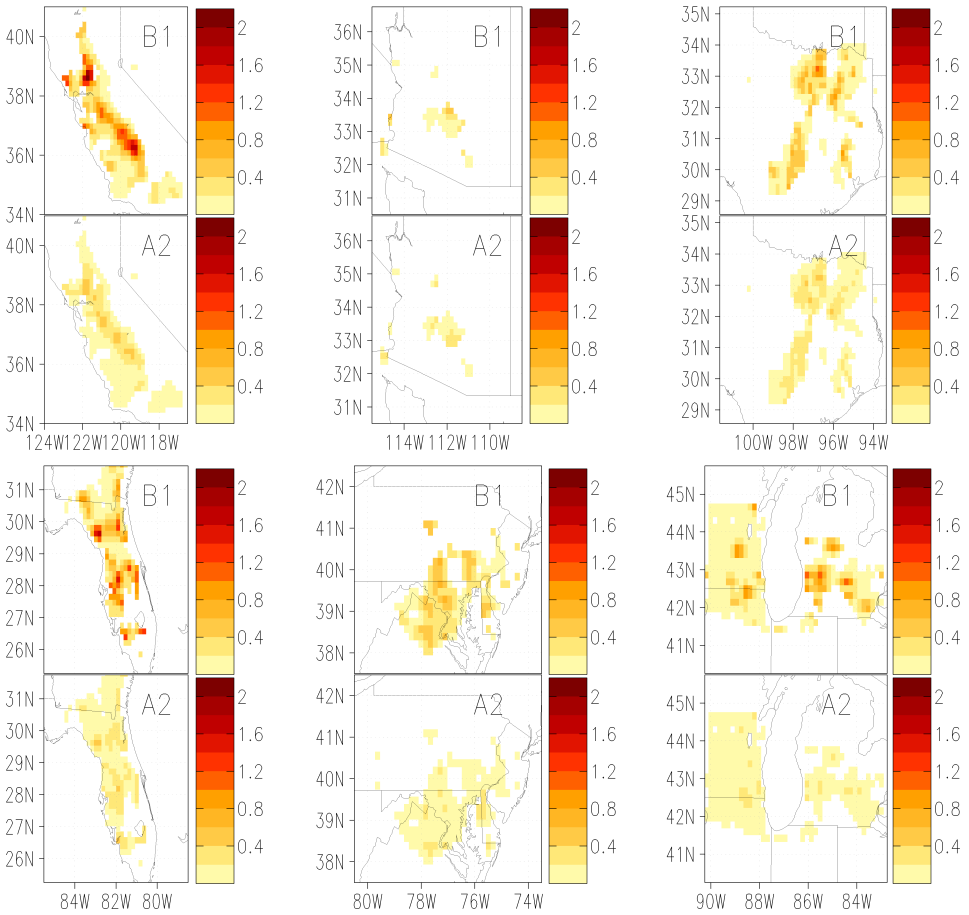

Fig. S16. As Figure 3 but for MAM.

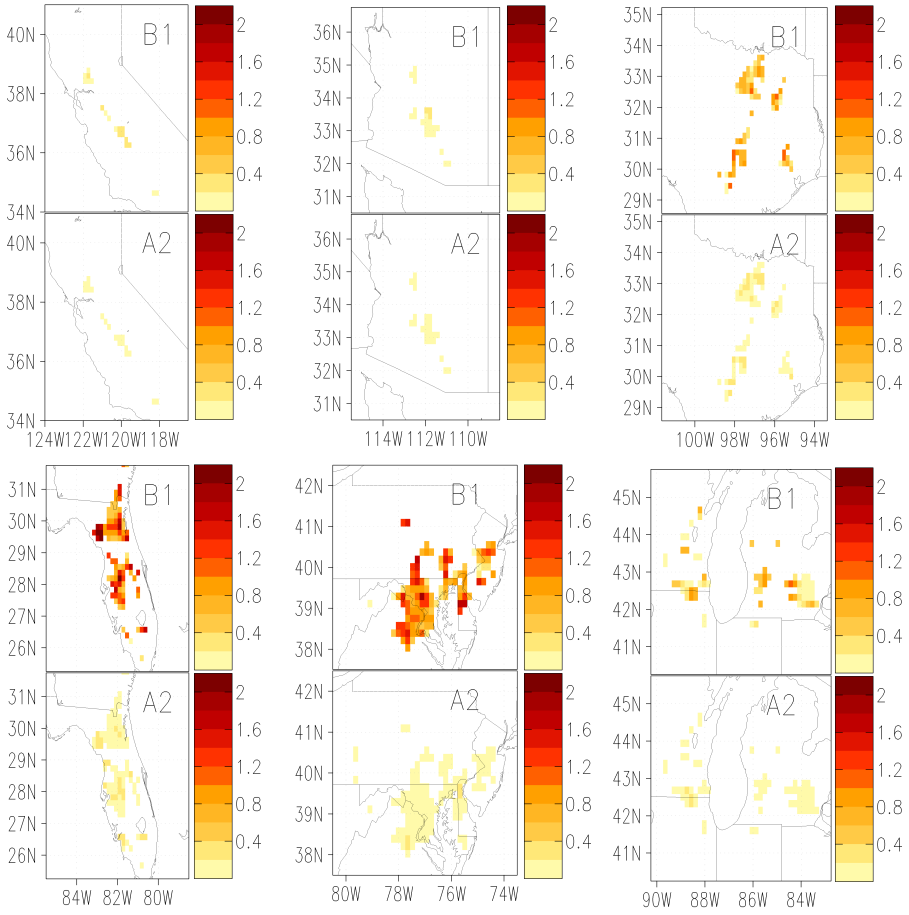

Fig. S17. As Figure 3 but for SON.

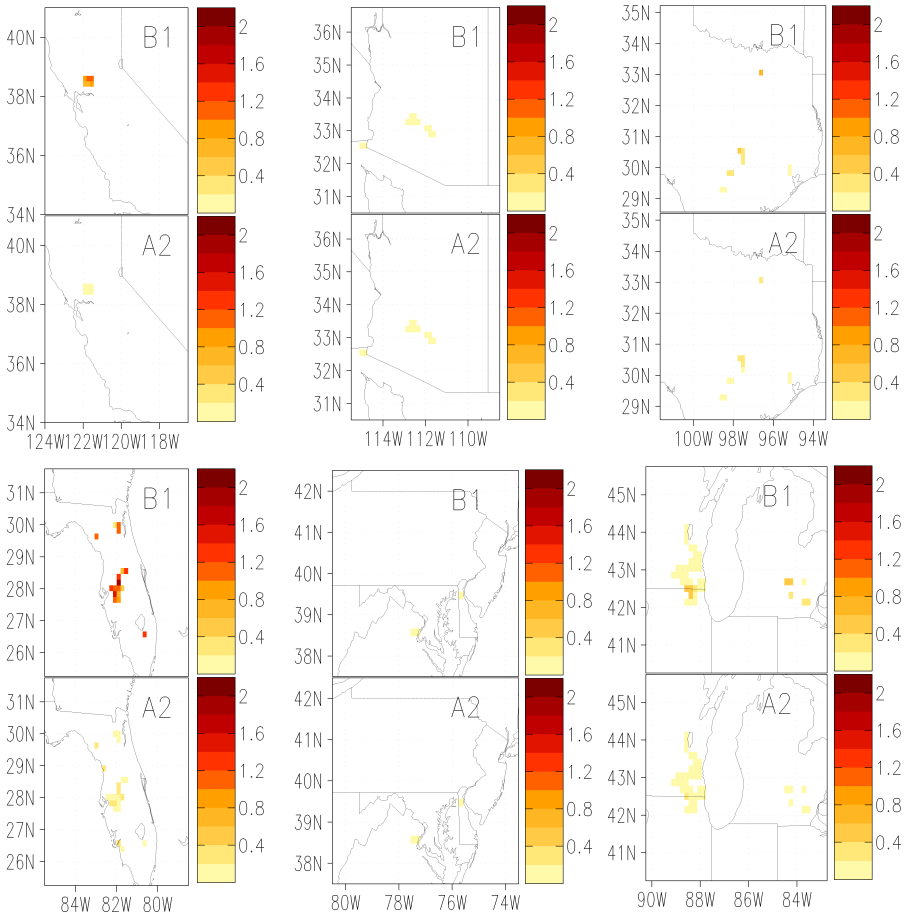

Fig. S18. As Figure 3 but for DJF.

Naming Convention	Spinup Period	Analysis Period
Control		
Control_1	JAN 2000 – DEC 2000	JAN 2001 – DEC 2008
Control_2	JUL 2000 – DEC 2000	JAN 2001 – DEC 2008
Control_3	–	JAN 2001 – DEC 2008
A2 ICLUS		
A2_1	JAN 2000 – DEC 2000	JAN 2001 – DEC 2008
A2_2	JUL 2000 – DEC 2000	JAN 2001 – DEC 2008
A2_3	–	JAN 2001 – DEC 2008
B1 ICLUS		
B1_1	JAN 2000 – DEC 2000	JAN 2001 – DEC 2008
B1_2	JUL 2000 – DEC 2000	JAN 2001 – DEC 2008
B1_3	–	JAN 2001 – DEC 2008
A2-GreenRoofs		
A2_GreenR1	JAN 2000 – DEC 2000	JAN 2001 – DEC 2008
A2_GreenR2	JUL 2000 – DEC 2000	JAN 2001 – DEC 2008
A2_GreenR3	–	JAN 2001 – DEC 2008
A2-CoolRoofs		
A2_CoolR1	JAN 2000 – DEC 2000	JAN 2001 – DEC 2008
A2_CoolR2	JUL 2000 – DEC 2000	JAN 2001 – DEC 2008
A2_CoolR3	–	JAN 2001 – DEC 2008
A2-GreenAlbedo		
A2_GreenAlb1	JAN 2000 – DEC 2000	JAN 2001 – DEC 2008
A2_ GreenAlb2	JUL 2000 – DEC 2000	JAN 2001 – DEC 2008
A2_ GreenAlb3	–	JAN 2001 – DEC 2008

Table S1. Naming convention of all experiments performed. **Control:** Control experiments, utilizing ICLUS urban representation for year 2000. **A2 ICLUS**: Experiments utilizing projected A2 ICLUS urban representation for year 2100. **B1 ICLUS**: Experiments utilizing projected B1 ICLUS urban representation for year 2100. **A2-GreenRoofs**: As A2 ICLUS experiments, with incorporation of green roofs for all urban areas. **A2-CoolRoofs**: As A2 ICLUS experiments, with incorporation of cool roofs for all urban areas. **A2-GreenAlbedo**: As A2 ICLUS experiments, with incorporation of reflective green roofs for all urban areas. All experiments were repeated 3 times (i.e., 3 ensemble members) with variable spinup time.

WRF Specifications

Model Version:	Version 3.2.1
Horizontal Grid:	ΔX, ΔY, 20-km
Number of Points:	310 (X-dir.); 200 (Y-dir.)
Vertical Levels:	30 levels
Initialization Time:	*See Table S1*
Terminal Time:	December 31, 21Z 2008
Analysis Time:	January 1, 00Z 2001 - December 31, 21Z 2008
ΔT:	90 seconds
Radiation Scheme:	RRTM (longwave); RRTMG (shortwave)
Surface Model:	Noah
Cumulus Scheme:	Kain-Fritsch
Microphysics Scheme	WSM-3
PBL Scheme	Mellor-Yamada-Janjic
Surface Layer	Eta similarity
Urban Model	3-category Urban Canopy Model
Initial and Lateral Boundary Conditions:	FNL

Table S2. Model parameterizations used for all experiments.

CALIFORNIA	**ΔT_{URB} [°C]; ΔT_{GHG} [°C]**	**ΔE_{URB} [%]; ΔE_{GHG} [%]**
A2	0.48; 4.26	− (1-7); − (13-64)
B1	0.31; 0.37	− (1-5); − (1-6)
Cool Roofs	-0.90	+ (3-14)
Green Roofs	0.14	− (0-2)
Green-Albedo Roofs	-0.90	+ (3-14)
ARIZONA		
A2 Scenario	0.54; 4.64	− (2-8); − (14-70)
B1 Scenario	-0.01; 0.36	− (0); − (1-5)
Cool Roofs	-0.79	+ (2-12)
Green Roofs	0.10	− (0-2)
Green-Albedo Roofs	-0.84	+ (3-13)
TEXAS		
A2	0.79; 4.27	− (2-12); − (13-64)
B1	0.24; 0.86	− (1-4); − (3-13)
Cool Roofs	-1.14	+ (3-17)
Green Roofs	0.16	− (0-2)
Green-Albedo Roofs	-1.18	+ (4-18)
FLORIDA		
A2	0.66; 3.46	− (2-10); − (10-52)
B1	0.38; 0.21	− (1-6); − (1-3)
Cool Roofs	-1.05	+ (3-16)
Green Roofs	0.01	− (0)
Green-Albedo Roofs	-1.03	+ (3-15)
MidAtlantic		
A2	0.59; 5.12	− (2-9); − (15-77)
B1	0.17; 1.58	− (1-3); − (5-24)
Cool Roofs	-1.54	+ (5-23)
Green Roofs	0.27	− (1-4)
Green-Albedo Roofs	-1.56	+ (5-23)
Chicago/Detroit		
A2	0.62; 6.78	− (2-9); − (20-102)
B1	0.27; 2.01	− (1-4); − (6-30)
Cool Roofs	-0.67	+ (2-10)
Green Roofs	0.59	− (2-9)
Green-Albedo Roofs	-0.63	+ (3-9)

Table S3. As Table 2 but for December-January-February (DJF).

Arizona			
Adaptation Strategy	Deployment %	JJA: ΔT_{URB} [°C]; ΔE_{URB} [%]	DJF: ΔT_{URB} [°C]; ΔE_{URB} [%]
Green Roofs	90%	-0.14; - (1-3)	0.09; - (0-1)
Cool Roofs	66%	-0.31; - (2-6)	-0.52; + (2-8)
Green-Albedo	57%	-0.46; - (2-9)	-0.48; + (1-7)

California			
Adaptation Strategy	Deployment %	JJA: ΔT_{URB} [°C]; ΔE_{URB} [%]	DJF: ΔT_{URB} [°C]; ΔE_{URB} [%]
Green Roofs	67%	-0.16; - (1-3)	0.09; - (0-1)
Cool Roofs	47%	-0.68; - (3-14)	-0.42; + (1-6)
Green-Albedo	44%	-0.73; - (4-15)	-0.40; + (1-6)

Chicago/Detroit			
Adaptation Strategy	Deployment %	JJA: ΔT_{URB} [°C]; ΔE_{URB} [%]	DJF: ΔT_{URB} [°C]; ΔE_{URB} [%]
Green Roofs	59%	-0.5; - (3-10)	0.35; - (1-5)
Cool Roofs	47%	-0.64; - (3-13)	-0.31; + (1-5)
Green-Albedo	45%	-0.67; - (3-13)	-0.28; + (1-4)

Florida			
Adaptation Strategy	Deployment %	JJA: ΔT_{URB} [°C]; ΔE_{URB} [%]	DJF: ΔT_{URB} [°C]; ΔE_{URB} [%]
Green Roofs	78%	-0.16; - (1-3)	0.01; - (0)
Cool Roofs	66%	-0.27; - (1-5)	-0.69; + (2-10)
Green-Albedo	62%	-0.29; - (1-6)	-0.64; + (2-10)

Mid-Atlantic			
Adaptation Strategy	Deployment %	JJA: ΔT_{URB} [°C]; ΔE_{URB} [%]	DJF: ΔT_{URB} [°C]; ΔE_{URB} [%]
Green Roofs	48%	-0.57; - (3-11)	0.13; - (0-2)
Cool Roofs	37%	-0.67; - (3-13)	-0.57; + (2-9)
Green-Albedo	34%	-0.69; - (3-14)	-0.53; + (2-8)

Texas			
Adaptation Strategy	Deployment %	JJA: ΔT_{URB} [°C]; ΔE_{URB} [%]	DJF: ΔT_{URB} [°C]; ΔE_{URB} [%]
Green Roofs	82%	-0.38; - (2-8)	0.13; - (0-2)
Cool Roofs	54%	-0.67; - (3-13)	-0.62; + (2-9)
Green-Albedo	50%	-0.73; - (4-15)	-0.59; + (2-9)

Table S4. As Table 2 but with urban adaptation deployment to a value that offsets urban-induced summertime warming.

References

1. Skamarock et al., "A description of the advanced research WRF version 3" (Natl. Cent. for Atmos. Res., Boulder, Colo., 2008).
2. Kusaka H., and Kimura F. (2004) Thermal effects of urban canyon structure on the nocturnal heat island: Numerical experiment using a mesoscale model coupled with an urban canopy model. *J. Appl. Meteorol.* 43: 1899–1910.
3. Georgescu M, Moustaoui M, Mahalov A, and Dudhia J. (2011) An alternative explanation of the semiarid urban area "oasis effect". *J. Geophys. Res.* 116(D24).
4. Sailor D J, and Lu L (2004) A top-down methodology for developing diurnal and seasonal anthropogenic heating profiles for urban areas. *Atmos. Environ.* 38: 2737–2748.
5. Bierwagen B G, Theobald D M, Pyke C R, Choate A, Groth P, et al. (2010) National housing and impervious surface scenarios for integrated climate impact assessments. *Proc. Natl. Acad. Sci. USA* 107: 20887-20892.
6. Csiszar I, and Gutman G (1999) Mapping global land surface albedo from NOAA AVHRR. *J. Geophys. Res.*, 104: 6215-6228.
7. Gutman G. and Ignatov A (1997) The derivation of green vegetation fraction from NOAA/AVHRR data for use in numerical weather prediction models. *Int. J. Remote Sensing* 19: 1533-1543.
8. Kumar R., and Kaushik S C (2005) Performance evaluation of green roof and shading for thermal protection of buildings. *Build. and Environ.* 40: 1505-1511.
9. Sailor D J (2008) A green roof model for building energy simulation programs. *Energy and Buildings* 40: 1466-1478.
10. EPA's Reducing Urban Heat Islands: Compendium of Strategies – Green Roofs. (2008). Available from: http://www.epa.gov/heatisland/resources/pdf/GreenRoofsCompendium.pdf
11. Carter T, and Keeler A. (2008) Life-cycle cost–benefit analysis of extensive vegetated roof systems. *Journal of Environmental Management* 87: 350-363.
12. Berndtsson C J (2010) Green roof performance towards management of runoff water quantity and quality: a review. *Ecological Engineering* 36: 351-360.
13. Li J F, Wai O W, Li Y S, Zhan J M, Ho Y A et al. (2010) Effect of green roof on ambient CO_2 concentration. *Building and Environment* 45: 2644-2651.
14. Castleton H F, Stovin V, Beck S B M, and Davison J B (2010) Green roofs: building energy savings and the potential for retrofit. *Energy and Buildings* 42: 1582-1591.
15. Susca T, Gaffin S R, and Dell'Osso G R (2011) Positive effects of vegetation: Urban heat island and green roofs. *Environmental Pollution* 159: 2119-2126.
16. Sun T, Bou-Zeid E, Wang Z H, Zerba E, and Ni G H (2013) Hydrometeorological determinants of green roof performance via a vertically-resolved model for heat and water transport. *Building and Environment* 60: 211-224.
17. EPA's Reducing Urban Heat Islands: Compendium of Strategies – Cool Roofs. (2008). Available from: http://www.epa.gov/heatisland/resources/pdf/CoolRoofsCompendium.pdf
18. Taha H (1996) Modeling impacts of increased urban vegetation on ozone air quality in the South Coast Air Basin. *Atmos. Env.* 30: 3423-3430.

19. Konopacki S, Akbari H, and Gartland L (1997) *Cooling energy savings potential of light-colored roofs for residential and commercial buildings in 11 US metropolitan areas* (No. LBNL--39433-Exec. Summ.). Lawrence Berkeley Lab., CA (US). Available at: http://www.osti.gov/scitech/servlets/purl/508151
20. Akbari H, Pomerantz M, and Taha H (2001) Cool surfaces and shade trees to reduce energy use and improve air quality in urban areas. *Solar Energy*, 70: 295-310.
21. Solecki W D, Rosenzweig C, Parshall L, Pope G, Clark M, Cox J et al. (2005) Mitigation of the heat island effect in urban New Jersey. *Global Environmental Change Part B: Environmental Hazards*, 6: 39-49.
22. Synnefa A, Santamouris M, and Apostolakis K (2070) On the development, optical properties and thermal performance of cool colored coatings for the urban environment. *Solar Energy* 81: 488-497.
23. Takebayashi H, and Moriyama M (2007) Surface heat budget on green roof and high reflection roof for mitigation of urban heat island. *Building and Environment* 42: 2971-2979.
24. Akbari H, Menon S, and Rosenfeld A (2009) Global cooling: increasing world-wide urban albedos to offset CO_2. *Climatic Change* 94: 275-286.
25. Oleson K W, Bonan G B, and Feddema J (2010) Effects of white roofs on urban temperature in a global climate model. *Geophys. Res. Lett.*, 37: L03701.
26. Georgescu M, Moustaoui M, Mahalov A, and Dudhia J (2013) Summer-time climate impacts of projected megapolitan expansion in Arizona. *Nat. Clim. Change* 3: 37- 41.
27. Li H, Harvey J T, Holland T J, Kayhanian M (2013) The use of reflective and permeable pavements as a potential practice for heat island mitigation and stormwater management. *Environ. Res. Lett.* 8: 015023.
28. Jacobson M Z, and Ten Hoeve J E (2012) Effects of urban surfaces and white roofs on global and regional climate. *J. Clim.* 25: 1028–1044.
29. Georgescu M, Mahalov A, and Moustaoui M (2012) Seasonal hydroclimatic impacts of Sun Corridor expansion. *Environ. Res. Lett.* 7: 034026-034035.
30. Ridgwell A, Singarayer J S, Hetherington A M, and Valdes P J (2009) Tackling regional climate change by leaf albedo bio-geoengineering. *Current Biology* 19: 146-150.
31. Shin, D-B, Kim J-H, and Park H-J (2011) Agreement between monthly precipitation estimates from TRMM satellite, NCEP reanalysis, and merged gauge-satellite analysis. *J. Geophys. Res.* 116: D16105.